American Journal of Sciences and Engineering Research www.iarjournals.com

American Journal of Sciences and Engineering Research
E-ISSN -2348 – 703X, Volume 4, Issue 2, 2021

Some Characteristics of a Wind Vortex

Sahoby LALAOHARISOA[1], Mbolahasina S. RALIJAONA[2], Jérôme VELO[3], Adolphe A. RATIARISON[4]

1 PhD student, Atmosphere, Climate and Oceans Dynamics Laboratory (DyACO), Physics and Applications, Sciences and Technologies Domain, University of Antananarivo, Madagascar.
2 Doctor, Atmosphere, Climate and Oceans Dynamics Laboratory (DyACO), Physics and Applications, Sciences and Technologies Domain, University of Antananarivo, Madagascar
3 University lecturer,Sciences and Technologies Domain, University of Toamasina, Madagascar.
4 Professor Emeritus, Atmosphere, Climate and Oceans Dynamics Laboratory (DyACO), Physics and Applications, Sciences and Technologies Domain, University of Antananarivo, Madagascar.

Abstract: *Air flow is a crucial parameter in many fields of application, especially in aerodynamics. The object of this article is the numerical simulation of a rotating airflow in a parallelepiped. The LES smagorinsky method, and the heat transfer equation under COMSOL were used. Simulations have shown that the number of Reynolds increases with altitude and initial rotation speed. The velocity field has a different direction at the domain front and the other remains rotating. The wind rose diagram showed the wind distribution and direction for each altitude. The most dominant values depend on each height.*

Keywords*: air in rotation, COMSOL Multiphysics, LES Smagorinsky, numerical simulation, wind rose*

I. Introduction

Rotating air masses are natural phenomena often found in nature. More precisely, it is observed on dry places and warmed by the sun's rays. This phenomenon is one of the stages of a dust devil. This can be illustrated in figures (1a) and (1b). The sun's rays heat the floor. The air above is heated (figure (1a)). The air starts to rotate under the effect of heat, creating a micro vacuum (figure (1b)).

(a) (b)

Figure 1: The first 2 stages of eddy formation according to Christophe MERTZ (meteorologist - ATMO-RISK):

The numerical method adopted is the Large-Eddy Simulation (LES) method. The objective of this work is to study the results obtained by a LES simulation in a rotating airflow for different values of the rotation speed.

 Received-16-03-2021, Accepted- 28-03-2021

The first part of our work consists of a representation of the system of equations and the method we used, as well as a brief introduction to the Comsol software. Then, the results obtained during the simulation will be shown on the second part. On the last part we will see the conclusion.

II. Material and method

✓ **Material [1]**

During this research, we used **COMSOL multiphysics 5.4** software. It is a numerical simulation software based on the finite element method, allowing to model a wide variety of physical phenomena characterizing a real problem.
The strong point of this software is to combine several physical phenomena during the same numerical simulation.
The physical interfaces that made this work possible are LES (Large-Eddy Simulation) Smagorinsky and heat transfer.

✓ **LES smagorinsky's method**

LES Smagorinsky is a turbulence model, used to simulate single-phase flows. This physical interface modifies the effect of small vortices and resolves large unstable vortices in three dimensions.
The equations solved by the LES Smagorinsky interface are the continuity equation for mass conservation and the Navier-Stokes equation, increased by a turbulent viscosity.

III. Mathematical model

We study the air flow in a square-based parallelepiped of 50 m side and 100 m height on figure (2).

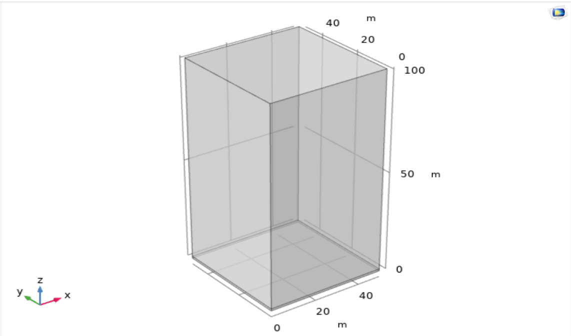

Figure 2: Field of Study

✓ **Filter function**

To separate small and large scales, Large Eddy simulation uses a low-pass filter, a Δ width G filter is introduced. The convolution product corresponding to the filtering of a variable $f\left(\vec{x},t\right)$ is written in physical space [2],[3]:

$$\overline{f}\left(\vec{x},t\right)=G*f\left(\vec{x},t\right)=\iiint_{\mathbb{R}^3} f\left(\vec{y},t\right)G\left(\vec{x}-\vec{y}\right)d\vec{y} \tag{0.1}$$

With $\overline{f}$: corresponds to scales greater than the width of the filter Δ.

$f^{'}$ is unknown and corresponds to size scales below Δ. It is defined in relation to the total field f by [4]:

$$f^{'}=f-\overline{f} \tag{0.2}$$

In this work our mesh is unstructured, the value of the width is therefore given by the following relation :

$$\Delta = \left(\Delta x \, \Delta y \, \Delta z\right)^{1/3} \tag{0.3}$$

Where $\Delta x, \Delta y \; et \, \Delta z$ are the steps of the meshes in the three directions of space.

Application of the Filter to the Navier Stokes Equation and Heat Transfer

The Navier Stokes equation for an incompressible Newtonian fluid is given by:

$$\nabla.\vec{u} = 0 \tag{0.4}$$

$$\frac{\partial \vec{u}}{\partial t} + \left(\vec{u}.\vec{\nabla}\right)\vec{u} - \nu \Delta \vec{u} + \frac{\vec{\nabla} P}{\rho} = \frac{\vec{f}}{\rho} \tag{0.5}$$

Assuming that the temperature field has no effect on the Navier stokes equation, the heat transfer equation is written:

$$\frac{\partial T}{\partial t} + \frac{\partial}{\partial x_j}\left(u_j T\right) = \frac{\partial}{\partial x_j}\left(\alpha_f \frac{\partial T}{\partial x_j}\right) + Q_f \tag{0.6}$$

Where α_j : the thermal diffusivity of the fluid

Q_f : Thermal Power Release Source Term

By applying the low-pass filter on the Navier Stokes equation, one obtains the equation to be solved in the LES approach.

Residual variables are :

$$\begin{aligned} u^{'} &= u - \bar{u}\,, \\ P^{'} &= P - \bar{P} \end{aligned} \tag{0.7}$$

Where $\bar{u}, \bar{P}$ are the variables to solve.

Under COMSOL, the filtered equation system is of the form :

$$\begin{aligned} &\rho \nabla.\left(u\right) = 0 \\ &\rho \frac{\partial u}{\partial t} + \overline{\rho\left(u.\nabla\right)u} = \nabla.\left[-PI + K\right] - \rho \nabla.\tau_{LES} \\ &K = \mu\left(\nabla u + \left(\nabla u\right)^T\right) \\ &\tau_{LES} = \overline{uu'^T} + \overline{u'u^T} + \overline{u'u'^T} \end{aligned} \tag{0.8}$$

K : stress tensor under mesh

τ_{LES} : Deformation Rate Tensor

μ :dynamic viscosity

And the heat transfer is :

$$\begin{aligned} &\rho C_P \frac{\partial T}{\partial t} + \rho C_p u.\nabla T + \nabla.q = Q + Q_p + Q_{vd} \\ &q = -k \nabla T \end{aligned} \tag{0.9}$$

ρ : density

Cp : specific heat capacity at constant pressure

T : absolute temperature

u : velocity vector

q : heat flux by conduction

Q : contains heat sources other than viscous dissipation

Q_{vd} :viscous dissipation in the fluid

IV. Results

On this present work, we vary the speed of rotation of the fluid, to have different values of the initial speed. We took 5 values of ω . The evolution of each physical parameter is observed for 10 seconds. The exploitation of the recovered data runs on Matlab.

- **Velocity field**

The following figure (3) shows the speed field at t=10s for a rotational speed of $\omega = \pi/35\, rad.s^{-1}$. At the edge the value is maximum with a direction of two different directions.

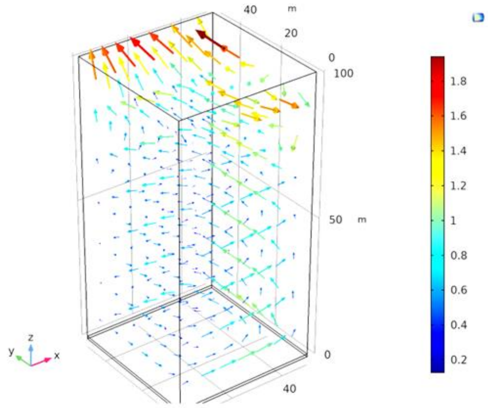

Figure 3: velocity field at t=10s

We took 3 shots of the domain (10 m, 60 m, 100 m), then we calculated the average speed on this shot (figure 4).

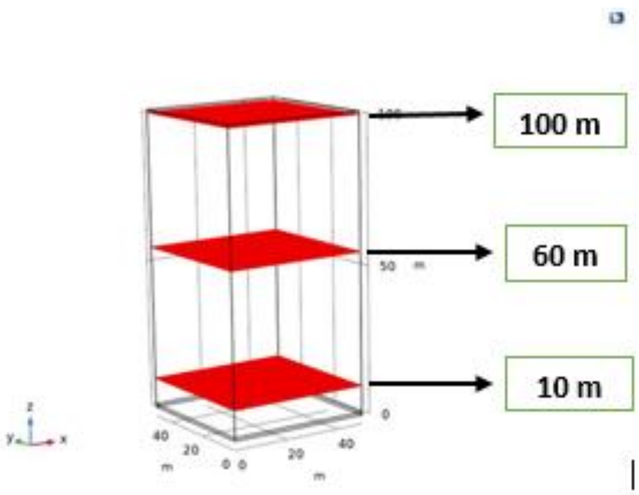

Figure 4 : 3 vertical plane section (10m, 60m, 100m)

The wind rose diagrams in the following figures show the distribution and direction of the wind at each z-height.

✓ At z=10m

The following figure (5) represents the wind rose at z=10 m at a speed of rotation $\omega = \pi/35\, rad.s^{-1}$.

In this figure, speeds 1m.s^{-1} are the most frequent. To the West, East, and South, we notice the presence of strong winds.

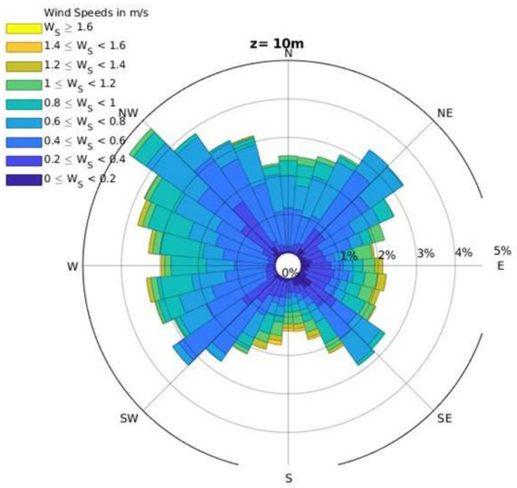

Figure 5: wind rose diagram at 10 m altitude

The most dominant proportion is in the Northwest with a percentage of 4.8% whose proportions of speed will be detailed in the following table.

Table 1: Proportion of prevailing wind at 10m

Velocity	Percentage
$0 \leq v_v < 0.2$ (m.s^{-1})	0,05
$0.2 \leq v_v < 0.4$ (m.s^{-1})	1,15
$0.4 \leq v_v < 0.6$ (m.s^{-1})	1,3
$0.6 \leq v_v < 0.8$ (m.s^{-1})	1,7
$0.8 \leq v_v < 1$ (m.s^{-1})	0,4
$1 \leq v_v < 1.2$ (m.s^{-1})	0,2
$1.2 \leq v_v < 1.4$ (m.s^{-1})	0

According to this table, speeds ranging from 0.6 m.s^{-1} to 0.8 m.s^{-1} are dominant for northwest winds.

- ✓ At z=60m

At an altitude of 60 m, the southwest wind is the most dominant with a proportion of 3.9%. Strong winds can be seen in the North, South, East and West (Figure(6)).

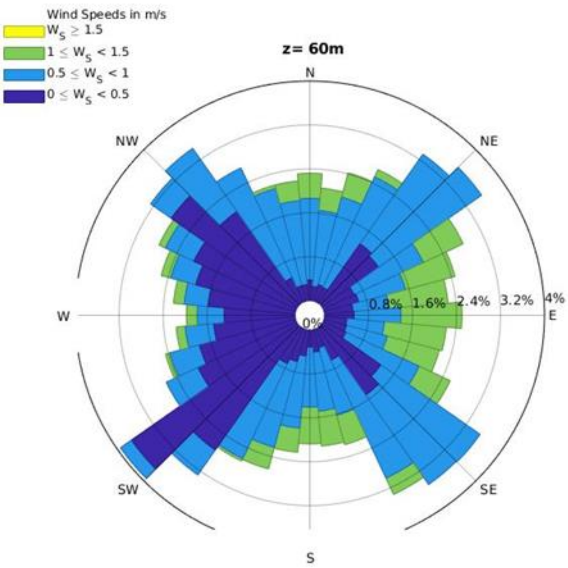

Figure 6: wind rose diagram at 60 m altitude

Wind speed distributions that have a proportion greater than 3.2% will be shown in the following table.

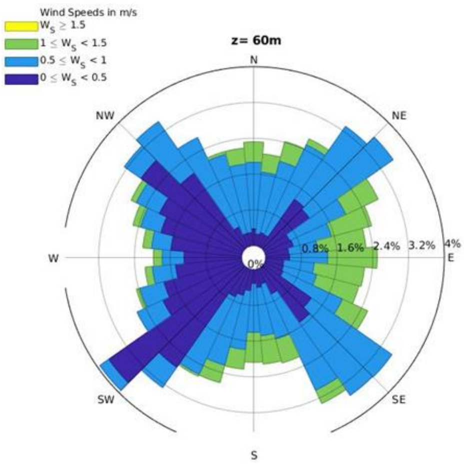

Figure 6: wind rose diagram at 60 m altitude

Wind speed distributions that have a proportion greater than 3.2% will be shown in the following table.

Table 2: Proportion of wind greater than 3.2% at 60m altitude

	North-East		South-East			South-West		North-West	
	3.6%	3,3%	3,4%	3,4%	3,3%	3,3%	3,95%	3,3%	3,6%
$0 \leq v_v < 0.5$ (m.s^{-1})	1,4	1,5	1	1,5	0,6	2,6	3,7	2,8	2
$0.5 \leq v_v < 1$ (m.s^{-1})	2,2	1,7	2,4	1,9	2,3	0,7	0,25	0,5	1,6
$1 \leq v_v < 1.5$ (m.s^{-1})	0	0	0	0	0,4	0	0	0	0

- ✓ At z=100m

The highest frequency is in the Northwest with 4.5%. Between north and northeast, a low proportion of high wind speed is observed. In the figure (7), speeds below 4m/s are the most frequent. The strong winds are between North and North-East.

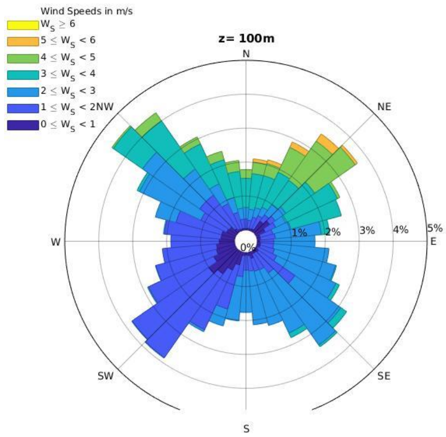

Figure 7: wind rose diagram at 100 m altitude

Frequency distributions for winds that have a proportion greater than 3% will be presented in the table below.

Table 3: Proportion of wind greater than 3% at 100m altitude

	North-East (%)		**South-East (%)**		**North-West (%)**				**South-West(%)**	
	3,7	3,6	3,4	3,2	4,4	4,5	3,1	3,05	3,6	3,8
$0 \le v_v < 1$ (m.s^{-1})	0,6	0,5	0,05	0,05	0,2	0,2	0,1	0,05	1	0,8
$1 \le v_v < 2$ (m.s^{-1})	0,3	0,2	0,75	1,55	1,1	1,1	0,95	0,85	2,6	3
$2 \le v_v < 3$ (m.s^{-1})	0,4	0,3	2,55	1,5	1	2,2	2	0,7	0	0
$3 \le v_v < 4$ (m.s^{-1})	0,9	0,9	0,05	0,2	1,8	0,95	0,05	1,1	0	0
$4 \le v_v < 5$ (m.s^{-1})	1,4	1,4	0	0	0,3	0,05	0	0,3	0	0
$5 \le v_v < 6$ (m.s^{-1})	0,1	0,3	0	0	0	0	0	0	0	0

The speeds $1 \le v_v < 2$ (m.s^{-1}) are most dominant at z=100 m.

- ✓ Reynolds Number

The calculation is done by meshing. We have different values of speed at each point so we get various very distinct Reynold numbers. It is calculated with the following formula:

$$\mathrm{Re} = \frac{\rho L U}{\mu} \qquad (0.10)$$

Where ρ : density of the fluid

L : characteristic length

U : velocity

μ : dynamic viscosity

A dimensional analysis shows that the Reynolds number is constructed to represent the ratio of convection forces to dissipation forces in a flow.

- ✓ Mean Reynolds number as a function of center altitude at t=10s for the rotation speed($\omega = \pi\ rad.s^{-1}, \omega = \pi/2\ rad.s^{-1}, \omega = \pi/4\ rad.s^{-1}, \omega = \pi/6\ rad.s^{-1}, \omega = \pi/35\ rad.s^{-1}$)

The curves in figure (8) below show the values of Re at t=10s in the center of the domain. The Reynolds number is of the order of 10^4, so the fluid flow is of the turbulent type. The speed variation of the Reynolds number depends on the altitude. Two maximum values are observed on the altitude 60m and 65m for a higher value of ω. As for that of a rotation speed $\omega = \pi/2\ rad.s^{-1}$, the Reynolds number is minimal at 78 m of altitude. For the three other values of ω the curves increase with altitude.

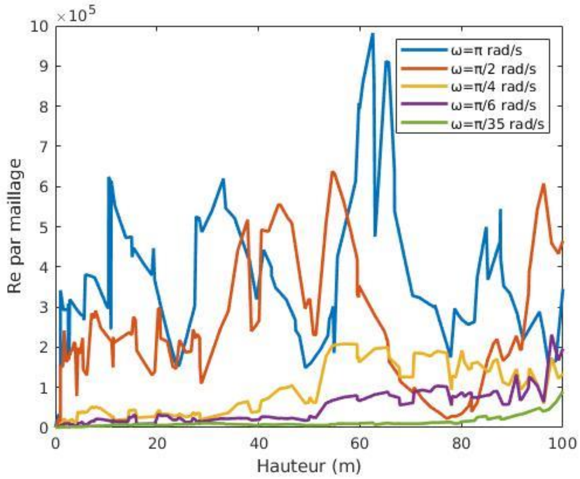

Figure 8: Reynolds numbers as a function of height for different values of ω

- ✓ Reynolds number on the horizontal at different altitude at t=10 s for rotation speed ($\omega = \pi\ rad.s^{-1}$, $\omega = \pi/2\ rad.s^{-1}$, $\omega = \pi/4\ rad.s^{-1}$, $\omega = \pi/6\ rad.s^{-1}$ $\omega = \pi/35\ rad.s^{-1}$)

- At z=10m

These figures represent the evolution of the Reynolds number on a horizontal line that cuts the center of the domain at z=10m. Its variation depends on the speed of rotation. At the center the value is minimal. These figures represent the evolution of the Reynolds number on a horizontal line that cuts the center of the domain at z=10m. Its variation depends on the speed of rotation. At the center the value is minimal. A maximum is observed between 40 to 50 m for a low rotation speed and 0 to 10 m for $\omega = \pi/6\ rad.s^{-1}$. The null values on both boundaries are due to the edge effect, it causes the Reynolds number in the center to decrease.

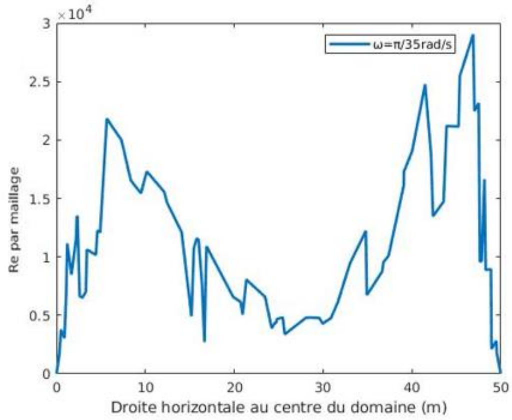

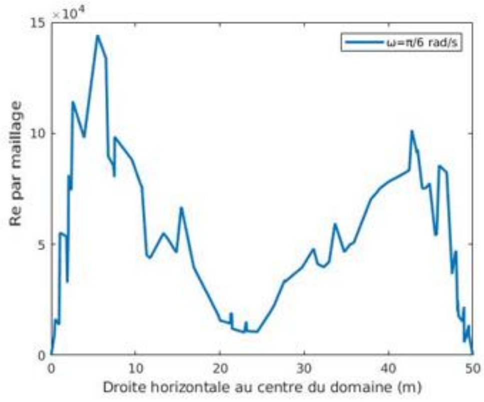

(a) (b)

Figure 1 : Reynolds number on a vertical line in the center of the domain at z=10m, (a) : $\omega = \pi/35\, rad.s^{-1}$, *(b) :* $\omega = \pi/6\, rad.s^{-1}$

For $\omega = \pi\, rad.s^{-1}$, $\omega = \pi/2\, rad.s^{-1}$ et $\omega = \pi/4\, rad.s^{-1}$, there are minimum values between 10m to 40m, but its position depends on the value of the rotation speed.

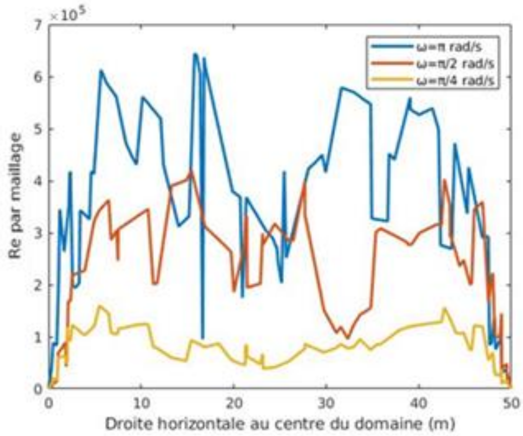

Figure 2: Reynolds number on a vertical line in the center of the domain at z=10m, for $\omega = \pi\ rad.s^{-1}$*,*

$\omega = \pi/2\, rad.s^{-1}$ *and* $\omega = \pi/4\, rad.s^{-1}$

- At z=50m

The following figures (11) represent the evolution of the Reynolds number as a function of the horizontal line in the center of the domain at 50 m altitude. The maximum value reached by Re varies according to the 5 values of ω. Comparing with the previous results, the minimum values intensify. The increase in the value of z to change the shape of our curve. For a low rotation speed (figure(11)), we observe an increase on some part of the line especially near the border. The maximum of the Reynolds number undergoes an increase of 10^5 for $\omega = \pi/6\, rad.s^{-1}$ with a displacement of 5m.

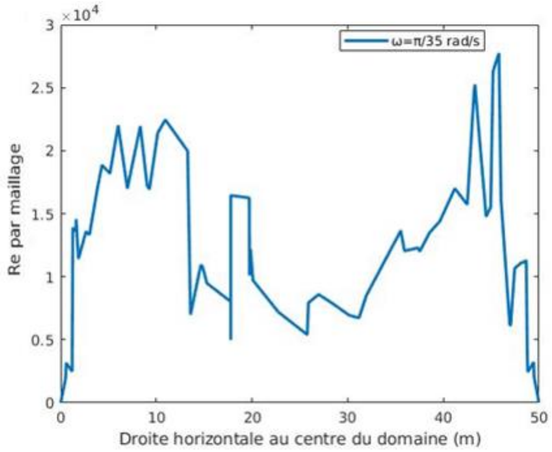

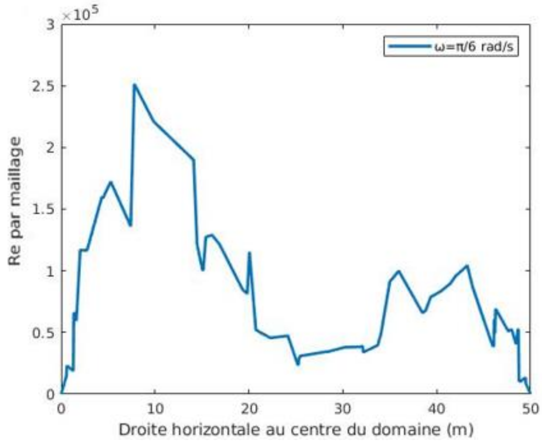

(a) *(b)*

Figure 11 : Reynolds numbers on a vertical line in the center of the domain at z=50m, (a) : $\omega = \pi/35\ rad.s^{-1}$*, (b) :* $\omega = \pi/6\ rad.s^{-1}$

The highest value is observed for a value of $\omega = \pi/2\ rad.s^{-1}$ (figure(12)). The minimums of three curves are between 15 m to 35 m.

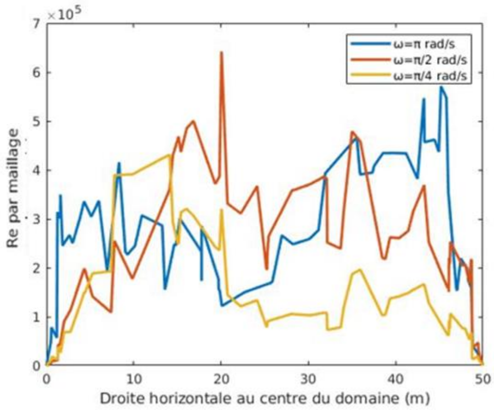

Figure 12: Reynolds number on a vertical line in the center of the domain at z=50m, for

$\omega = \pi\ rad.s^{-1}$, $\omega = \pi/2\ rad.s^{-1}$ *et* $\omega = \pi/4\ rad.s^{-1}$

The following figures (13a, 13b, 14) show the evolution of the Reynolds number as a function of the horizontal line in the center at z=100m for different values of ω. The value of Re becomes maximum in the center for all ω. The increase in Reynolds number is due to the opening of the domain on the front, which influenced the wind.

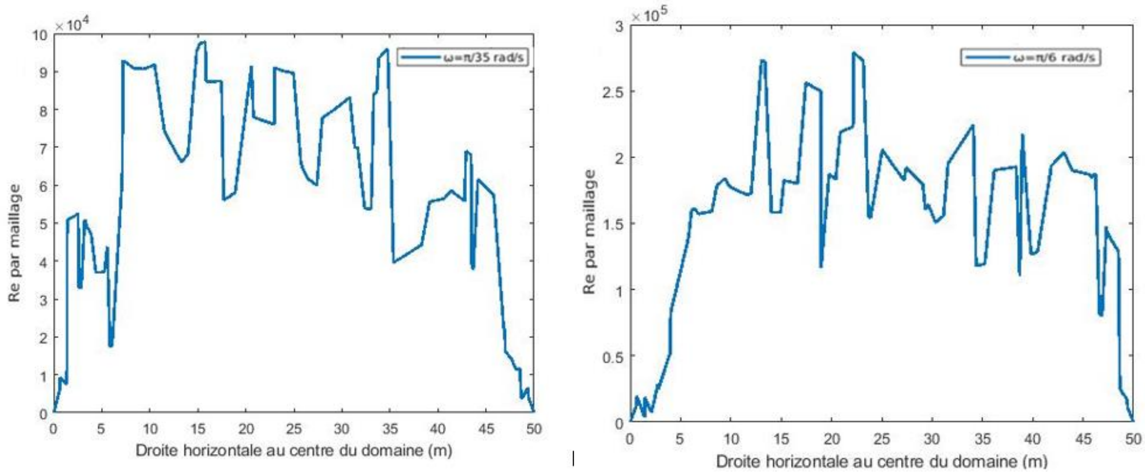

(a) (b)

Figure 13: Reynolds number on a vertical line in the center of the domain at z=100m,(a) : $\omega = \pi/35\, rad.s^{-1}$ *,*

(b) : $\omega = \pi/6\, rad.s^{-1}$

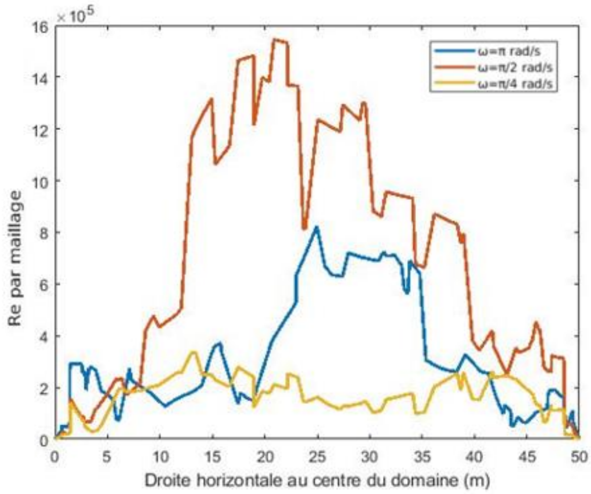

Figure 14: Reynolds number on a vertical line in the center of the domain at z=100m, for

$\omega = \pi\, rad.s^{-1}$, $\omega = \pi/2\, rad.s^{-1}$ *et* $\omega = \pi/4\, rad.s^{-1}$

V. Conclusion

This work concerns the study of the results obtained by the LES smagorinsky method of simulating rotating air in a parallelepiped. From the results retrieved during 10 s of simulation, we were able to plot the wind-rose diagram for different altitudes, calculating the average speed for ω low. He showed that the direction and distribution of the average wind speed depends on the altitude. The 5 values of ω that were initially imposed on an influence on the Reynolds numbers obtained during the simulation. The latter is of the order of 10^4 for the low values of ω and of the order of 10^5 for the other values. This means that the flow is of the turbulent type. The value of Re increases as the altitude increases. For the continuation of our work we will study the influence of the rotation speed on other physical parameters, in order to better understand the studied phenomenon.

VI. Bibliography

1. https://www.comsol.com/
2. LEONARD, A. Energy cascade in Large-Eddy Simulations of turbulent fluid flows. Adv. Geophys. 18A (1974), 237–248.
3. Andrés E. Tejada-Martinez, Dynamic subgrid-scale modeling for large-eddy simulation of turbulent flows with a stabilized finite element method, November 2002, Polytechnic Institute Troy, New York
4. Simulation des Grandes Echelles d'écoulements turbulents avec transferts de chaleur, Alexandre Chatelain, 7 septembre 2004, Institut national Polytechnique de Grenoble